

Polarization multistates in composite ferroelectrics

Chuhan Tang,¹ Zhiqiang Tian,¹ Tao Ouyang,² Anlian Pan,^{3,1} and Mingxing Chen^{1,4}

¹*Key Laboratory for Matter Microstructure and Function of Hunan Province,
Key Laboratory of Low-Dimensional Quantum Structures and Quantum Control of Ministry of Education,
School of Physics and Electronics, Hunan Normal University, Changsha 410081, China*

²*Hunan Key Laboratory for Micro-Nano Energy Materials and Device and School of Physics and Optoelectronics,
Xiangtan University, Xiangtan 411105, Hunan, China*

³*Key Laboratory for Micro-Nano Physics and Technology of Hunan Province,
College of Materials Science and Engineering, Hunan University, Changsha 410082, China*

⁴*State Key Laboratory of Powder Metallurgy, Central South University, Changsha 410083, China**

(Dated: March 19, 2024)

Going beyond the bistability paradigm of the charge polarizations in ferroelectrics is highly desired for ferroelectric memory devices toward ultra-high density information storage. Here, we propose to build multistates in composite ferroelectrics, which have both the intrinsic and sliding-induced polarizations. We illustrate the concept in H-stacking bilayers of 1T^{''} transition-metal dichalcogenides by first-principle calculations. We find that there are at least one order of magnitude difference in the energy barriers between these two types polarizations, which suggests that the external electric fields required to flipping them are significantly different. This difference allows for a novel flipping mechanism involving layer sliding and layer-by-layer flipping for the transforming of the polarization states. As a result, sextuple switchable states can be achieved for the 1T^{''} bilayers by properly controlling electric field. Our study provides a new route to design polarization multistates for developing next-generation memory devices.

I. INTRODUCTION

Ferroelectrics have promising applications in non-volatile memory devices with high-storage density, fast read/write speed, and low power consumption [1, 2]. There has been a growing demand for continuously increasing the storage density of the ferroelectric (FE) devices in the era of big data. For this purpose, the thickness of the Ferroelectrics has to be reduced. Unfortunately, conventional perovskite ferroelectrics suffer from the problem that the ferroelectricity is suppressed as the film thickness is decreased to a critical value due to the depolarization field [3–5].

Two-dimensional (2D) ferroelectrics have advantages in addressing the scaling issue due to the fact that they have no dangling bonds at the surfaces. Up to date, a great number of 2D ferroelectrics have been experimentally indentified and theoretically predicted [6–15]. For instance, it was experimentally shown that the ultrathin films of rhombohedral SnTe exhibits unexpectedly much higher Curie temperatures than its bulk phase [6]. Theoretical calculations predicted that monolayers of the orthorhombic group-IV monochalcogenides also exhibit ferroelectricity with the in-plane polarizations and high Curier temperatures [7]. Interestingly, a few groups of 2D ferroelectrics with the out-of-plane polarizations (OOP), e.g., In₂Se₃ and CuMP₂S₆ (M = In and Cr) were recently found by both theoretical predictions and experiments [12–14, 16–20]. Moreover, ferroelectricity with the OOP was also found in the distorted 1T phases of transition-metal chalcogenides (TMD) [21–24]. Such a

kind of ferroelectricity is highly desired for their applications in FE devices.

In addition to the intrinsic 2D ferroelectricity, it was shown that stacking nonpolar monolayers into bilayers and multilayers can also give rise to simultaneous polarization [25–32]. This property is due to the electronic reconstruction caused by stacking-induced symmetry breaking, for which the interlayer sliding is responsible for the reversal of the polarizations.

In this study, we propose to design polarization multistates by combining both the intrinsic and sliding ferroelectricity in composite ferroelectrics, which are derived by stacking of certain two-dimensional ferroelectrics. These systems have one more degree of freedom for switching the polarizations than any of the individual counterparts. As a result, there are eight polarization states for bilayers. We further illustrate the concept in bilayers of 1-T^{''} TMD by performing first-principle calculations. We find that six of them can be achieved by properly controlling the external electric field, which is based on the fact that the energy barrier for the layer sliding is much smaller than those for the intrinsic counterpart. Moreover, the sextuple polarization states exhibit different electronic structures. Therefore, they can be distinguished by the tunneling current across the FE tunnel junctions. Our study provides a new way to design novel polarization states for ultrahigh-density storage technology that goes beyond the conventional FE devices.

* mxchen@hunnu.edu.cn

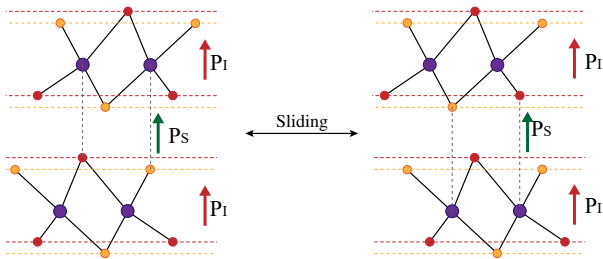


FIG. 1. Sketch of polarization multistates in composite ferroelectrics, which exhibit both intrinsic and stacking-induced polarizations. The former (P_I) originates from the motion of ions within the layers. Whereas the later (P_S) is dependent on specific stacking. There are eight polarization states for their combination in a bilayer. (a, b) show two of them for a bilayer with distorted 1T phase (ferroelectric) in the H-stacking. (c-h) schematically show the others

II. RESULTS AND DISCUSSION

A. Model and concept

Our concept makes use of the intrinsic polarizations (P_I) due to ionic motions and those induced by stacking, which is depicted in Fig. 1. For intrinsic 2D ferroelectrics such as CuInP_2S_6 and In_2Se_3 , their bilayers have four different polarization configurations. Two of them have opposite polarizations but both are in the interlayer FE coupling. The other two have interlayer antiferroelectric (AFE) couplings, which are in the tail-to-tail and tail-to-tail configurations, respectively. While for the sliding ferroelectricity, the polarization is strongly dependent on the stacking order. For instance, for the H phase of TMD layers without inversion, R-stacking gives rise to net electronic polarizations, which is absent for the H-stacking. Whereas for the T phase, it requires the H-stacking for nonvanishing polarizations. In both stackings that induce polarizations, the key is the staking of the metal atoms in the one layer onto the nonmetal atoms in the other layer. This property gives rise to the bistability nature of the stacking-induced polarizations (P_S) for the bilayers. However, combining these two types of ferroelectricity in one system, which is named composite ferroelectrics in this study, may give rise to a much larger number of states for their thin films. Fig. 1 depicts that there are octuple polarization states for a bilayer in composite ferroelectrics.

One important feature of this kind of ferroelectrics is that the energy barriers for switching the intrinsic spontaneous polarizations are generally much larger than those for the interlayer slidings. For instance, it is about 66 meV for In_2Se_3 monolayer [12] and about 218 meV for CuInP_2S_6 monolayer [33]. Whereas the energy barriers for layer sliding in the bilayer of h-BN is only about 9 meV [25]. Thus, there is at least one order of magnitude difference in the energy barriers between the two different ferroelectrics. As a result, one can expect that

the external electric fields for switching them have the same trend. Namely, small electric fields are needed for switching P_S . Whereas much larger electric fields are required to flip P_I . Thus, in such composite ferroelectrics, the transforming of the two types of polarizations can be achieved by properly controlling the electric field.

B. Material realization

We find that the bilayers of distorted TMD in the d1T and 1T $''$ phases by appropriate stackings are potential candidates for the proposed multistates. These phases are derived from a $\sqrt{3} \times \sqrt{3}$ and a 2×2 structural reconstructions of the 1T phase, respectively. In these phases, the Mo atoms have in-plane displacements. For instance, for the 1T $''$ phase three of them form a contracted triangle, which in turn leads to an expanded triangle (see Fig. 2). As a result, the chalcogen atoms sitting the hollow site of the contracted triangles have an out-of-plane displacement relative to those on the hollow sites of the expanded ones. Such displacements gives rise to the out-of-plane polarizations for the d1T and 1T $''$ -TMD phases, which have been confirmed by experiments [22, 24]. The energy barriers for the ferroelectric transforming from the nudged elastic band (NEB) calculations [34, 35] are 212 meV, 271 meV, and 306 meV for 1T $''$ - MoS_2 , MoSe_2 , and MoTe_2 , respectively.

Despite the structural reconstruction, the stacking order that is responsible for sliding ferroelectricity still appears in the corresponding stacking of the 1T $''$ bilayers. Therefore, there are stacking-induced polarizations for them. Like the standard sliding ferroelectrics, proper shiftings of the 1T $''$ -TMD layers can lead to the reverse of the stacking-induced polarization.

To validate our idea, we have performed first-principles calculations for the H-stacking bilayers of 1T $''$ - MoX_2 ($X = \text{S}, \text{Se}, \text{and Te}$) using the Vienna Ab initio Simulation Package [36]. The exchange-correlation functional is parametrized using the Perdew–Burke–Ernzerhof (PBE) formalism in the generalized gradient approximation [37]. The pseudopotentials were constructed by the projector augmented wave method [38, 39]. Van der Waals dispersion forces between the adsorbate and the substrate were accounted by using the DFT-D3 method [40]. A 12×12 Monkhorst-Pack k -mesh was used to sample the two-dimensional Brillouine zone and a plane-wave energy cut off of 400 eV was used for structural relaxation and self-consistent calculations.

We have performed systematic calculations for various configurations of the H-stacking 1T $''$ - MoX_2 bilayer. In Fig. 2, the cell of the 1T $''$ -TMD is represented by a parallelogram with blue lines, where the cells of the 1T phase are denoted by the black lines. Therefore, there are six nonequivalent stackings [Figs. 2(c-j)] for a 1T $''$ bilayer with respect to the H-stacking of the unreconstructed 1T phase. Our calculations find that they are all energy local minimums. Among them S2 has the lowest energy

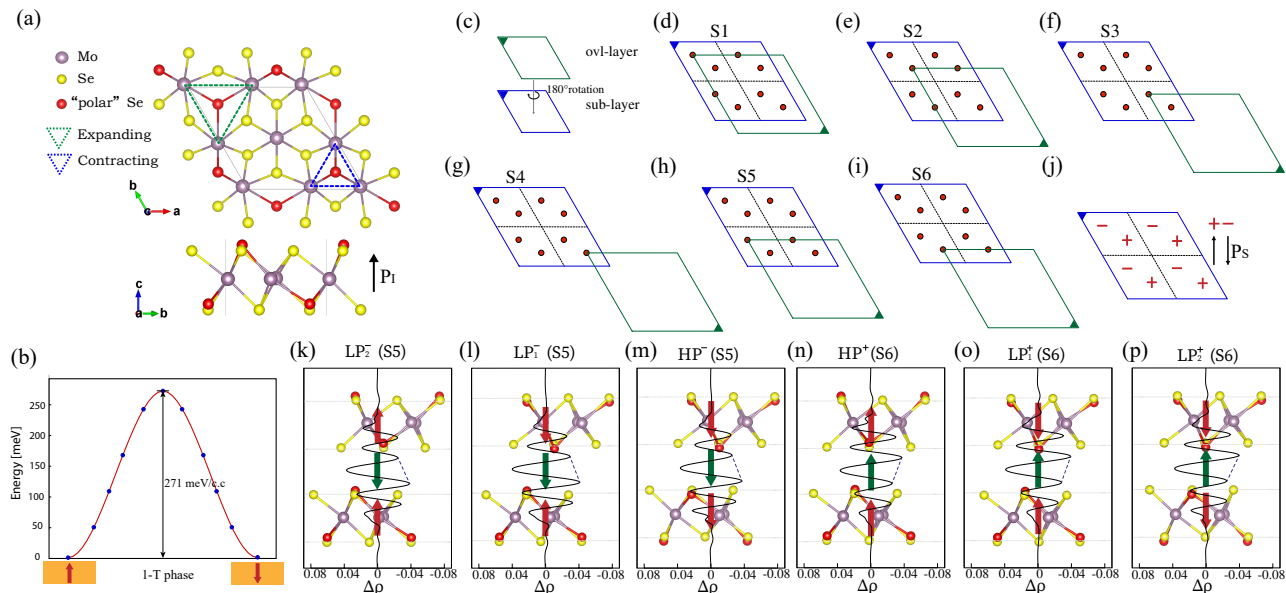


FIG. 2. Polarization multistates in a $1T''$ -MoSe₂ bilayer. (a) Geometric structure of the $1T''$ -TMD monolayer, which is derived from a 2×2 supercell of the $1T$ phase. (b) The energy barrier for reversing the polarizations in the $1T''$ -MoSe₂ monolayer. (c-i) The stacking configurations of the H-stacking $1T''$ -TMD bilayer. The cells for the $1T$ phase are denoted by dashed parallelograms. (j) The signs of P_S for the stackings show in (d-i). (k-l) Polarizations for S5 and S6 in different interlayer couplings. P_I and P_S are denoted by red and green arrows, respectively. $\Delta\rho(z)$ denotes planar average of charge density difference.

for the ferroelectric interlayer coupling, i.e., $\uparrow\uparrow$, where the polarizations of the individual layers are shown by arrows. The energy differences between them are small (~ 20 meV). The stacking-induced polarizations P_S are calculated by subtracting those of the individual layers from the total polarization. The signs of P_S for the eight configurations are shown in Fig. 2g, which can be classified into two groups with opposite signs, i.e., $\{S1, S3, S5\}$ and $\{S2, S4, S6\}$.

We have performed calculations of the possible polarization states for the two groups. Below we only show three of them for S5 and S6, which are shown in Fig. 2. The one with tail-to-tail interlayer coupling is not shown since it is absent for the transforming discussed below. The calculated polarizations are listed in Table 1. Our results find that the sign of P_S for each stacking remains unchanged regardless of the interlayer polarization coupling. There are only slight changes in the magnitude of P_S with respect to different interlayer polarization couplings for each stacking. This property can be understood since the stacking order remains unchanged, although the interlayer polarization coupling varies. Consequently, the electronic reconstruction is preserved. We have performed analysis of the differential charge density ($\Delta\rho$) by subtracting the change density of the individual layers from that of the bilayer, which is shown in Fig. 2. The results confirm the electronic origin and clearly explain the signs of P_S for all the stackings.

TABLE I. Polarization states for S5 and S6. P_I^T and P_I^B (PC/m) denote the intrinsic polarizations in the top and bottom layers, respectively. $P_I^T - P_I^B$ represent the interlayer polarization configurations. P_{tot} denotes the total polarization (pC/m).

Stacking	$P_I^T - P_I^B$	P_{tot}	P_I^T	P_I^B	P_S
S5	$\uparrow\uparrow$	-0.18	0.18	0.20	-0.56
	$\downarrow\downarrow$	-0.69	-0.23	-0.17	-0.29
	$\uparrow\downarrow$	-0.48	0.16	-0.17	-0.46
	$\downarrow\uparrow$	-0.69	-0.21	0.21	-0.69
S6	$\uparrow\uparrow$	0.69	0.17	0.22	0.30
	$\downarrow\downarrow$	0.20	-0.20	-0.17	0.57
	$\uparrow\downarrow$	0.45	0.18	-0.17	0.44
	$\downarrow\uparrow$	0.69	-0.22	0.22	0.69

C. Transforming of the polarization multistates

We now discuss the transforming of the polarization multistates. The energy barriers between the configurations are shown in Fig. 3. There are three pathways for S2 to transform when its P_S is flipped, i.e., S2-S1, S2-S3, and S2-S5, respectively. The barrier for the pathway from S2 to S1 is about 71 meV, which is slightly higher than that for the one from S2 to S5. The pathway from S2 to S3 has an energy barrier of about 325 meV. Therefore, the pathway from S2 to S5 is favored when an external electric field is imposed to switch P_S . Based on the above trend, there two pathways with low energy barriers for S5 and S6 to transform, i.e., S5-S2 and S5-S6, respectively.

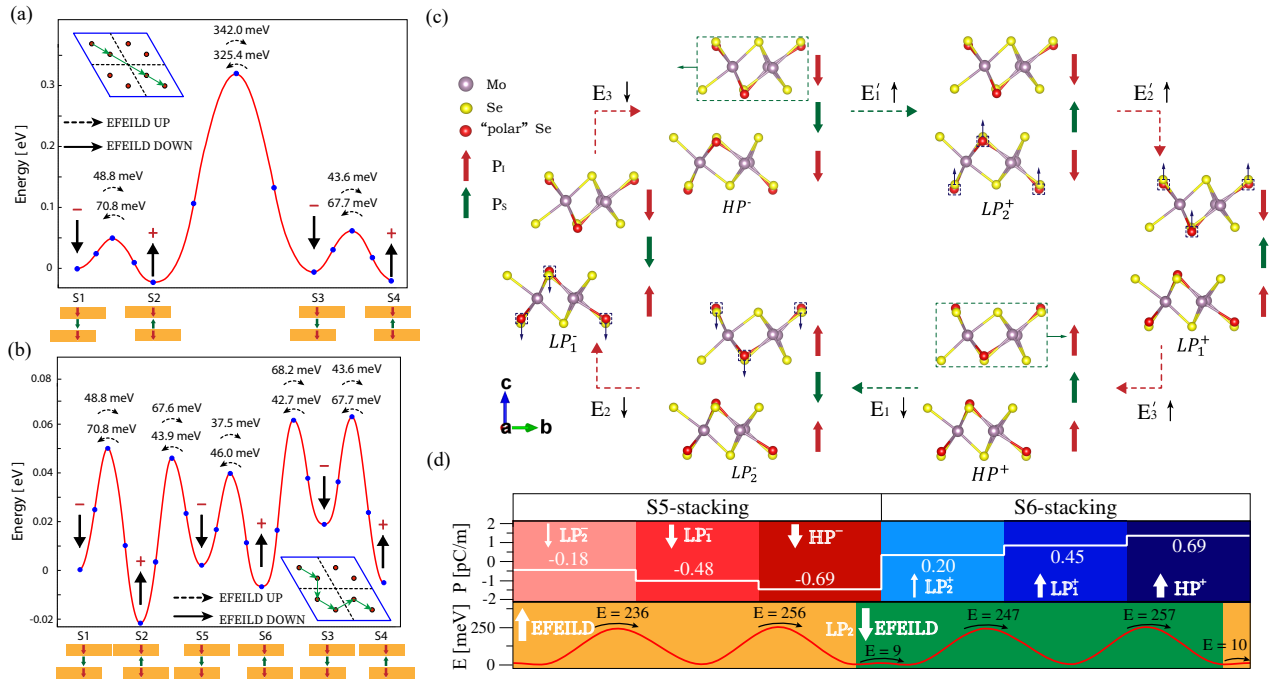


FIG. 3. Transforming of the polarization multistates in a ferroelectric $1T''$ -TMD bilayer. Energy barriers for the pathways (a) S1-S2-S3-S4 and (b) S1-S2-S5-S6-S3-S4, respectively, which are also shown in the insets. Here we only show the barriers for the layers with downward intrinsic polarizations. Others show the same trend. The polarization configuration is shown below the label for each stacking. (c) Transforming of the sextuple polarization states that can be achieved by external electric fields. (d) The net polarizations for the multistates and the energy barriers for the pathways between them.

The energy barriers for them are about 38 meV and 44 meV, respectively. For S6, the energy barriers are about 46 and 68 meV for the pathways from it to S5 and to S3, respectively. The trends in the energy barrier for the investigated pathways suggest that the system prefers to be transformed between S5 and S6 as P_S is switched by sliding.

Assuming the system is in the lowest energy structure S2 with all downward polarizations, which can be achieved by polling, an electric field E_1 antiparallel to the polarizations can flip its P_S by layer sliding so that the system is transformed into LP_2^- . This state is in the stacking order S5. Then, a much larger electric field (E_2) than E_1 can be used to flipping the intrinsic polarizations within the layers. Note that the two layers are symmetrically distinct. Therefore, the electric fields required to flip their polarizations are different (see Fig. 3). This difference leads to a layer-selective flipping mechanism for this kind of systems. Our calculations find that the energy barriers for flipping the top layer is 20 meV lower than the that for the bottom layer for LP_2^- . So, the polarizations of the top layer is prior to be flipped. By this operation, the system is transformed into the state LP_1^- (see Fig. 3). Then, an electric field (E_3) larger than E_2 can be used to flip the polarizations of the bottom layer. Note that the energy difference in the barriers for switching P_S within the layers is comparable to that for the layer sliding. Therefore the difference between E_3 and E_2 is

expected to be comparable to E_1 .

The system is now in the state HP^- , which have all the intrinsic and the stacking-induced polarizations parallel to the external electric field. Likewise, reversing the electric field properly can yield another three polarization states, which are named LP_2^+ , LP_1^+ , and HP^+ , respectively. Therefore, there are sextuple polarization states, which can be achieved by controlling the external electric field. Note that there are only three (two) states can be achieved for the bilayers of intrinsic (sliding) ferroelectrics. Thus, combining these two kinds of ferroelectricity can double or triple the number of states compared to those solely having one ingredient. Moreover, these states have different electronic structures due to the different polarization properties, i.e., band gap and band edges. Therefore, they can be distinguished by the tunneling current across it FE tunnel junctions. Given that R-stacking $1T''$ -TMD thin films were already obtained by experiments [24], the systems in H-stacking proposed by the present study are expected to be experimentally feasible once the $1T''$ -TMD monolayers have been exfoliated.

III. CONCLUSIONS

In summary, we have proposed to combine the intrinsic and sliding ferroelectricities in one material, i.e., the

composite ferroelectrics, which can be obtained by proper stackings of two-dimensional ferroelectrics. We find that this concept can be illustrated in 1T^{''}-TMD bilayers using first-principles calculations. Our NEB calculations reveal that a mechanism involving layer sliding and layer-by-layer flipping can give rise to six switchable states by controlling external electric fields. We anticipate that more states can be obtained for thicker films. Our results show that this strategy allows significantly increasing the number of polarization states for ultra-high density information storage. The unusual polarization states are also expected to provide opportunities of designing novel electronic devices and manipulating the electronic properties

of overlayers in heterostructures.

ACKNOWLEDGMENTS

This work was supported by the National Natural Science Foundation of China (Grants No. 12174098, No. U19A2090, and No. 52372260) and Project supported by State Key Laboratory of Powder Metallurgy, Central South University, Changsha, China. Calculations were carried out in part using computing resources at the High Performance Computing Platform of Hunan Normal University.

-
- [1] J. F. Scott, Applications of Modern Ferroelectrics, *Science* **315**, 954 (2007).
- [2] L. W. Martin and A. M. Rappe, Thin-film ferroelectric materials and their applications, *Nat. Rev. Mater.* **2**, 1 (2016).
- [3] J. Junquera and P. Ghosez, Critical thickness for ferroelectricity in perovskite ultrathin films, *Nature* **422**, 506 (2003).
- [4] D. D. Fong, G. B. Stephenson, S. K. Streiffer, J. A. Eastman, O. Auciello, P. H. Fuoss, and C. Thompson, Ferroelectricity in ultrathin perovskite films, *Science* **304**, 1650 (2004).
- [5] M. Dawber, K. Rabe, and J. Scott, Physics of thin-film ferroelectric oxides, *Rev. Mod. Phys.* **77**, 1083 (2005).
- [6] K. Chang, J. Liu, H. Lin, N. Wang, K. Zhao, A. Zhang, F. Jin, Y. Zhong, X. Hu, W. Duan, Q. Zhang, L. Fu, Q.-K. Xue, X. Chen, and S.-H. Ji, Discovery of robust in-plane ferroelectricity in atomic-thick SnTe, *Science* **353**, 274 (2016), <https://www.science.org/doi/pdf/10.1126/science.aad8609>.
- [7] R. Fei, W. Kang, and L. Yang, Ferroelectricity and Phase Transitions in Monolayer Group-IV Monochalcogenides, *Phys. Rev. Lett.* **117**, 097601 (2016).
- [8] N. Higashitarumizu, H. Kawamoto, C.-J. Lee, B.-H. Lin, F.-H. Chu, I. Yonemori, T. Nishimura, K. Wakabayashi, W.-H. Chang, and K. Nagashio, Purely in-plane ferroelectricity in monolayer SnS at room temperature, *Nat. Commun.* **11**, 1 (2020).
- [9] K. Chang, F. Küster, B. J. Miller, J.-R. Ji, J.-L. Zhang, P. Sessi, S. Barraza-Lopez, and S. S. P. Parkin, Microscopic Manipulation of Ferroelectric Domains in SnSe Monolayers at Room Temperature, *Nano Lett.* **20**, 6590 (2020).
- [10] Z. Guan, Y. Zhao, X. Wang, N. Zhong, X. Deng, Y. Zheng, J. Wang, D. Xu, R. Ma, F. Yue, Y. Cheng, R. Huang, P. Xiang, Z. Wei, J. Chu, and C. Duan, Electric-Field-Induced Room-Temperature Antiferroelectric-Ferroelectric Phase Transition in van der Waals Layered GeSe, *ACS Nano* **16**, 1308 (2022).
- [11] X.-Y. Ma, H.-Y. Lyu, K.-R. Hao, Y.-M. Zhao, X. Qian, Q.-B. Yan, and G. Su, Large family of two-dimensional ferroelectric metals discovered via machine learning, *Sci. Bull.* **66**, 233 (2021).
- [12] W. Ding, J. Zhu, Z. Wang, Y. Gao, D. Xiao, Y. Gu, Z. Zhang, and W. Zhu, Prediction of intrinsic two-dimensional ferroelectrics in In₂Se₃ and other III₂-VI₃ van der Waals materials, *Nat. Commun.* **8**, 1 (2017).
- [13] Y. Zhou, D. Wu, Y. Zhu, Y. Cho, Q. He, X. Yang, K. Herrera, Z. Chu, Y. Han, M. C. Downer, H. Peng, and K. Lai, Out-of-Plane Piezoelectricity and Ferroelectricity in Layered α -In₂Se₃ Nanoflakes, *Nano Lett.* **17**, 5508 (2017).
- [14] C. Cui, W.-J. Hu, X. Yan, C. Addiego, W. Gao, Y. Wang, Z. Wang, L. Li, Y. Cheng, P. Li, X. Zhang, H. N. Alsharief, T. Wu, W. Zhu, X. Pan, and L.-J. Li, Intercorrelated In-Plane and Out-of-Plane Ferroelectricity in Ultrathin Two-Dimensional Layered Semiconductor In₂Se₃, *Nano Lett.* **18**, 1253 (2018).
- [15] J. Gou, H. Bai, X. Zhang, Y. L. Huang, S. Duan, A. Ariando, S. A. Yang, L. Chen, Y. Lu, and A. T. S. Wee, Two-dimensional ferroelectricity in a single-element bismuth monolayer, *Nature* **617**, 67 (2023).
- [16] A. Belianinov, Q. He, A. Dziaugys, P. Maksymovych, E. Eliseev, A. Borisevich, A. Morozovska, J. Banys, Y. Vysochanskii, and S. V. Kalinin, CuInP₂S₆ room temperature layered ferroelectric, *Nano Lett.* **15**, 3808 (2015).
- [17] F. Liu, L. You, K. L. Seyler, X. Li, P. Yu, J. Lin, X. Wang, J. Zhou, H. Wang, H. He, S. T. Pantelides, W. Zhou, P. Sharma, X. Xu, P. M. Ajayan, J. Wang, and Z. Liu, Room-temperature ferroelectricity in CuInP₂S₆ ultrathin flakes, *Nat. Commun.* **7**, 12357 (2016).
- [18] W. F. Io, S.-Y. Pang, L. W. Wong, Y. Zhao, R. Ding, J. Mao, Y. Zhao, F. Guo, S. Yuan, J. Zhao, J. Yi, and J. Hao, Direct observation of intrinsic room-temperature ferroelectricity in 2D layered CuCrP₂S₆, *Nat. Commun.* **14**, 7304 (2023).
- [19] Y. Ma, Y. Yan, L. Luo, S. Pazos, C. Zhang, X. Lv, M. Chen, C. Liu, Y. Wang, A. Chen, Y. Li, D. Zheng, R. Lin, H. Algaidi, M. Sun, J. Z. Liu, S. Tu, H. N. Alsharief, C. Gong, M. Lanza, F. Xue, and X. Zhang, High-performance van der Waals antiferroelectric CuCrP₂S₆-based memristors, *Nat. Commun.* **14**, 7891 (2023).
- [20] X. Wang, Z. Shang, C. Zhang, J. Kang, T. Liu, X. Wang, S. Chen, H. Liu, W. Tang, Y.-J. Zeng, J. Guo, Z. Cheng, L. Liu, D. Pan, S. Tong, B. Wu, Y. Xie, G. Wang, J. Deng, T. Zhai, H.-X. Deng, J. Hong, and J. Zhao, Electrical and magnetic anisotropies in van der Waals multiferroic CuCrP₂S₆, *Nat. Commun.* **14**, 840 (2023).
- [21] S. N. Shirodkar and U. V. Waghmare, Emergence of Ferroelectricity at a Metal-Semiconductor Transition in a 1T

- Monolayer of MoS₂, *Phys. Rev. Lett.* **112**, 157601 (2014).
- [22] S. Yuan, X. Luo, H. L. Chan, C. Xiao, Y. Dai, M. Xie, and J. Hao, Room-temperature ferroelectricity in MoTe₂ down to the atomic monolayer limit, *Nature Communications* **10**, 1775 (2019).
- [23] J.-H. Choi and S.-H. Jhi, Origin of robust out-of-plane ferroelectricity in d1T-MoS₂ monolayer, *Journal of Physics: Condensed Matter* **32**, 045702 (2019).
- [24] A. Lipatov, P. Chaudhary, Z. Guan, H. Lu, G. Li, O. Cregut, K. D. Dorkenoo, R. Proksch, S. Cherifi-Hertel, D.-F. Shao, E. Y. Tsymbal, J. Iniguez, A. Sinitskii, and A. Gruverman, Direct observation of ferroelectricity in two-dimensional MoS₂, *npj 2D Materials and Applications* **6**, 1 (2022).
- [25] L. Li and M. Wu, Binary compound bilayer and multilayer with vertical polarizations: two-dimensional ferroelectrics, multiferroics, and nanogenerators, *ACS Nano* **11**, 6382 (2017).
- [26] Z. Fei, W. Zhao, T. A. Palomaki, B. Sun, M. K. Miller, Z. Zhao, J. Yan, X. Xu, and D. H. Cobden, Ferroelectric switching of a two-dimensional metal, *Nature* **560**, 336 (2018).
- [27] M. Wu and J. Li, Sliding ferroelectricity in 2D van der Waals materials: Related physics and future opportunities, *Proceedings of the National Academy of Sciences* **118**, e2115703118 (2021).
- [28] M. Vizner Stern, Y. Waschitz, W. Cao, I. Nevo, K. Watanabe, T. Taniguchi, E. Sela, M. Urbakh, O. Hod, and M. Ben Shalom, Interfacial ferroelectricity by van der Waals sliding, *Science* **372**, 1462 (2021).
- [29] X. Wang, K. Yasuda, Y. Zhang, S. Liu, K. Watanabe, T. Taniguchi, J. Hone, L. Fu, and P. Jarillo-Herrero, Interfacial ferroelectricity in rhombohedral-stacked bilayer transition metal dichalcogenides, *Nat. Nanotechnol.* , 1 (2022).
- [30] Y. Wan, T. Hu, X. Mao, J. Fu, K. Yuan, Y. Song, X. Gan, X. Xu, M. Xue, X. Cheng, C. Huang, J. Yang, L. Dai, H. Zeng, and E. Kan, Room-Temperature Ferroelectricity in 1T'-ReS₂ Multilayers, *Phys. Rev. Lett.* **128**, 067601 (2022).
- [31] J. Ji, G. Yu, C. Xu, and H. J. Xiang, General Theory for Bilayer Stacking Ferroelectricity, *Phys. Rev. Lett.* **130**, 146801 (2023).
- [32] L. Yang, S. Ding, J. Gao, and M. Wu, Atypical Sliding and Moiré Ferroelectricity in Pure Multilayer Graphene, *Phys. Rev. Lett.* **131**, 096801 (2023).
- [33] G. Yu, A. Pan, and M. Chen, Interface engineering of ferroelectricity in thin films of thiophosphate ABP_2X_6 ($A = \text{Cu, Ag}; B = \text{In, Bi, Cr, V}; X = \text{S, Se}$), *Phys. Rev. B* **104**, 224102 (2021).
- [34] G. Henkelman, B. P. Uberuaga, and H. Jónsson, A climbing image nudged elastic band method for finding saddle points and minimum energy paths, *J. Chem. Phys.* **113**, 9901 (2000).
- [35] G. Henkelman and H. Jónsson, Improved tangent estimate in the nudged elastic band method for finding minimum energy paths and saddle points, *J. Chem. Phys.* **113**, 9978 (2000).
- [36] G. Kresse and J. Furthmüller, Efficient iterative schemes for ab initio total-energy calculations using a plane-wave basis set, *Phys. Rev. B* **54**, 11169 (1996).
- [37] J. P. Perdew, K. Burke, and M. Ernzerhof, Generalized Gradient Approximation Made Simple, *Phys. Rev. Lett.* **77**, 3865 (1996).
- [38] P. E. Blöchl, Projector augmented-wave method, *Phys. Rev. B* **50**, 17953 (1994).
- [39] G. Kresse and D. Joubert, From ultrasoft pseudopotentials to the projector augmented-wave method, *Phys. Rev. B* **59**, 1758 (1999).
- [40] S. Grimme, J. Antony, S. Ehrlich, and H. Krieg, A consistent and accurate ab initio parametrization of density functional dispersion correction (DFT-D) for the 94 elements H-Pu, *J. Chem. Phys.* **132**, 154104 (2010).